Article:

Shi, Y., Ma, S., Zhao, Y. et al. (2 more authors) (2023) A Physics-Informed Low-Shot Adversarial Learning For sEMG-Based Estimation of Muscle Force and Joint Kinematics. IEEE Journal of Biomedical and Health Informatics. ISSN 2168-2194

https://doi.org/10.1109/jbhi.2023.3347672

This article has been accepted for publication in IEEE Journal of Biomedical and Health Informatics. This is the author's version which has not been fully edited and content may change prior to final publication. Citation information: DOI 10.1109/JBHI.2023.3347672

A Physics-Informed Low-Shot Adversarial Learning For sEMG-Based Estimation of Muscle Force and Joint Kinematics

Yue Shi, Shuhao Ma, Yihui Zhao, Chaoyang Shi, and Zhiqiang Zhang

***Abstract*— Muscle force and joint kinematics estimation from surface electromyography (sEMG) are essential for real-time biomechanical analysis of the dynamic interplay among neural muscle stimulation, muscle dynamics, and kinetics. Recent advances in deep neural networks (DNNs) have shown the potential to improve biomechanical analysis in a fully automated and reproducible manner. However, the small sample nature and physical interpretability of biomechanical analysis limit the applications of DNNs. This paper presents a novel physics-informed low-shot adversarial learning method for sEMG-based estimation of muscle force and joint kinematics. This method seamlessly integrates Lagrange's equation of motion and inverse dynamic muscle model into the generative adversarial network (GAN) framework for structured feature decoding and extrapolated estimation from the small sample data. Specifically, Lagrange's equation of motion is introduced into the generative model to restrain the structured decoding of the high-level features following the laws of physics. A physics-informed policy gradient is designed to improve the adversarial learning efficiency by rewarding the consistent physical representation of the extrapolated estimations and the physical references. Experimental validations are conducted on two scenarios (i.e. the walking trials and wrist motion trials). Results indicate that the estimations of the muscle forces and joint kinematics are unbiased compared to the physics-based inverse dynamics, which outperforms the selected benchmark methods, including physics-informed convolution neural network (PI-CNN), vallina generative adversarial network (GAN), and multi-layer extreme learning machine (ML-ELM).**

***Index Terms*— muscle force and joint kinematics, surface Electromyographic, low-shot learning, generative adversarial network, physics-informed optimization, mode collapse**

I. Introduction

HUMAN movements involve complex interactions within the neuromuscular system. The estimation of muscle force and joint kinematics dynamics provides detailed biomechanical analysis to understand the human neuromuscular system [1], [2], which benefits high-level exoskeleton control in human–robot interaction (HRI) applications, such as sports rehabilitation [3], [4] and human augmentation [5], [6]. In biomechanical engineering, the joint kinetics and kinematics generated by muscle contraction affect the flexibility and efficiency of human locomotion [7]. How to estimate muscle force and joint kinematics accurately and reproducibly has become an important research target in biomechanics.

However, the high flexibility of human locomotion determines that it is difficult to establish the model accurately, especially involving interactive joint kinetics and kinematics dynamics [8]. This challenge directly affects the efficiency and feasibility of biomechanical engineerings, such as human-exoskeleton cooperative control, in real-world scenarios [9]. As one of the myoelectric signals, surface electromyography (sEMG), which can be captured easily from human skin, have been proven effective to high-precision estimation of joint kinetics and kinematics [10]. It augments the cognitive synergy between human and robotic entities [11]. Therefore, the correlation between sEMG signals and the exerted force/locomotion deserves to be comprehensively investigated.

There are many existing physics-based models developed to establish the forward and inverse relationship between the sEMG signals and the joint kinetics and kinematics to interpret transformation among neural excitations and muscle dynamics [12], [13]. These forward-inverse dynamics-based approaches estimate the continuous muscle force and joint kinematics through the sEMG-driven muscle activation dynamics, muscle contraction dynamics, and musculoskeletal geometry. For example, Pau *et al* [14] introduced a combined approach using a simplified geometric and musculoskeletal model to predict continuous elbow joint movement. Hashemi *et al* [15] achieved precision muscle force estimations through the integration of angle-based sEMG amplitude calibration with parallel cascade identification, experimental outcomes indicate that their method yields a reduced estimation error rate during dynamic muscle contractions. Huang *et al* [16] gathered sEMG signals utilizing a high-density electrode grid and employed the non-negative matrix factorization algorithm for the joint kinetics estimation. Although such physics-based models explicitly explain and map sEMG signals to joint kinematics, the high cost of their static optimization has always limited the practical applications of these models [17], [18].

Recently, deep neural networks (DNNs) have provided an alternative solution to map the sEMG signals to the joint kinetics and kinematics [19], [20]. In this kind of model,

Yue Shi, Zhiqiang Zhang, Shuhao Ma are with the School of Electronic and Electrical Engineering, University of Leeds, Leeds, UK. LS2 9JT (e-mail: y.shi1@leeds.ac.uk, z.zhang3@leeds.ac.uk, elsma@leeds.ac.uk), Corresponding author: Zhiqiang Zhang.

Yihui Zhao is with Bristol Robotic Lab, University of Bristol, Bristol, UK. (e-mail: yihui.zhao@bristol.ac.uk).

Chaoyang Shi is with the School of Mechanical Engineering, Tianjin University. (e-mail: chaoyang.shi@tju.edu.cn).

This article has been accepted for publication in IEEE Journal of Biomedical and Health Informatics. This is the author's version which has not been fully edited and content may change prior to final publication. Citation information: DOI 10.1109/JBHI.2023.3347672

the multi-layer convolution architecture has been explored to establish relationships between movement variables and neuromuscular status [21], [22]. For example, Nasr et al [23] mapped the sEMG signals to the regression of joint angle, joint velocity, joint acceleration, joint torque, and activation torque, illustrating that the multi-layer convolution operators are capable of extracting underlying motor control information. Zhang et al [22] developed an active deep convolutional neural network to enhance the dynamic tracking capability of the musculoskeletal model on unseen data.

Despite the advantages, traditional DNNs are data-hungry and their performance is highly dependent on the quantity and quality of data [24]. Meanwhile, biomechanics analysis is typically a physics-based extrapolation process with small sample nature [25], [26]. Therefore, it is a challenge to train DNNs with small sample data so that the DNNs perform consistently with the physics-based model. To fill this research gap, the low-shot learning (LSL) technique has attracted many researchers' attention [27]–[29]. For example, Rahimian *et al* [30] introduced a Few-Shot Learning Hand Gesture Recognition (FS-HGR) model to enhance the generalization capability of DNNs from a limited number of instances. Lehmler *et al* [31] explored a low-shot learning methodology that adjusts DNNs to new users with only a small size of training data.

In addition, the generative adversarial network (GAN) framework has shown great potential in handling physical extrapolating and predictive problems [21], [32], [33]. The GAN-based model is capable of discovering the structured patterns of the references and extrapolating the underlying data distribution characteristics during the adversarial learning process [34]. For example, Chen *et al* [35] tested and evaluated the performance of the deep convolutional generative adversarial network (DCGAN) on sEMG-based data enhancement, and their results indicated that the extrapolated data is able to augment the diversity of the original data. Fahimi *et al* [36] proposed a generative adversarial learning framework for generating artificial electroencephalogram (EEG) data to extrapolate the brain-computer interface, and their findings suggest that generated EEG augmentation can significantly improve brain-computer interface performance.

In this study, we propose a physics-informed low-shot adversarial learning method for muscle force and joint kinematics estimation from multi-channel sEMG signals. This method seamlessly integrates physics knowledge with the GAN framework for structured feature decoding and extrapolated estimation from the small sample data. Specifically, Lagrange's equation of motion is introduced into the generative model to restrain the structured decoding of the high-level features following the laws of physics. And a physics-informed policy gradient is designed to improve the low-shot adversarial learning efficiency by rewarding the consistent physical representation of the extrapolated estimations and the physical references. Results show the muscle forces and joint kinematics prediction from the proposed method are environment-adaptive and unbiased compared to the ground truth measurement.

The remainder of this paper is organized as follows: Section II detailed describes the algorithm of the proposed physics-informed policy gradient for reinforcement generative adversarial learning, including the mathematics framework of the algorithm and network architectures. Section III presents the material and experimental methods. Section IV discusses the experimental results and model evaluations. and Section V presents the conclusions.

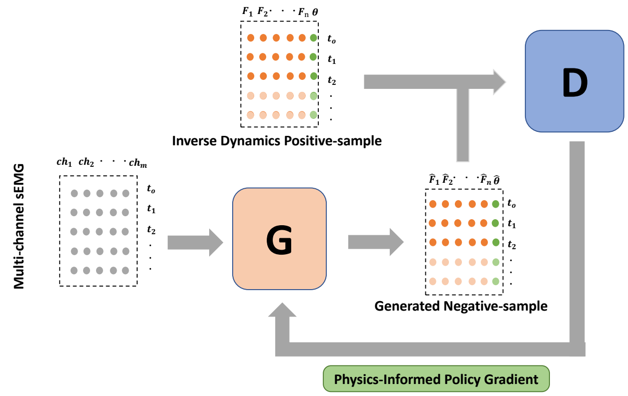

Fig. 1. The main architecture of the proposed physics-informed low-shot generative adversarial learning for muscle force and joint kinematics prediction from multi-channel sEMG time-series

II. Physics-Informed Low-Shot Adversarial Learning Method

The continuous estimation of muscle forces (F) and joint kinematics(θ) from multi-channel sEMG can be denoted as the time-series generation problem. Thus, given a real multi-channel sEMG time series, we train a σ parameterized generative network G_σ to estimate the muscle force ($\hat{F}$) and joint kinematics ($\hat{\theta}$). In this section, we propose a GAN framework, as shown in Fig.1, to train the G_σ on the small sample data. Specifically, we denote the G_σ estimated $\hat{F}$ and $\hat{\theta}$ as the negative samples (see details in Section II-B), the ground truth θ and the inverse dynamics-based F [37] as positive samples (i.e. references). The ϕ-parameterized discriminative model D_ϕ is introduced to distinguish the positive samples and negative samples (see details in Section II-C). During adversarial learning, the task of D_ϕ is to determine if an input sample is positive or negative, and the task of G_σ is to generate the unbiased negative samples to fool the discriminator D_ϕ. The model optimization process is driven by the newly proposed physics-informed policy gradient (see details in Section II-A) which rewards the homogeneity of physics representation and structural characteristics between the positive and negative samples.

A. GAN optimization via physics-informed policy gradient

The physics-informed policy gradient method, inspired by reinforcement learning [38], aims to optimize the learning process of the GAN-based model yielding physical extrapolations from the small sample data (i.e. low-shot learning). Mathematically, the physics-informed policy gradient method maximizes its expected reward $J(\sigma)$ based on the physics law and structured characteristics from the small sample data. The $J(\sigma)$ consists of two parts, the structural reward R_{G_σ} and

This article has been accepted for publication in IEEE Journal of Biomedical and Health Informatics. This is the author's version which has not been fully edited and content may change prior to final publication. Citation information: DOI 10.1109/JBHI.2023.3347672

physics representation action $Q_{D(\phi)}^{G(\sigma)}$. The $J(\sigma)$ is defined as follows.

$$\begin{aligned} J(\sigma) &= \mathbb{E}[R_{G_\sigma}(G_\sigma(sEMG_{0:T}))] \\ &\quad \cdot Q_{D\phi}^{G\sigma}((G_\sigma(sEMG_{0:T}), [F,\theta]_{0:T}) \\ &= \mathbb{E}[R_{G_\sigma}([\hat{F},\hat{\theta}]_{0:T})] \\ &\quad \cdot Q_{D\phi}^{G\sigma}([\hat{F},\hat{\theta}]_{0:T}, [F,\theta]_{0:T}) \end{aligned} \tag{1}$$

where $sEMG_{0:T}$ is the input multi-channel sEMG time series for T time steps. The $J(\sigma)$ is beginning with the expected reward from a predetermined state from the positive samples. And then, the R_{G_σ} and $Q_{D(\phi)}^{G(\sigma)}$ will jointly optimize the generative network G_σ to generate the unbiased $([\hat{F},\hat{\theta}]_{0:T})$ following the physics laws.

Specifically, the structural reward R_{G_σ} is computed by the G_σ and defined as follows.

$$R_G(([\hat{F},\hat{\theta}]_{0:T}) = \exp^{PL^2([\hat{F},\hat{\theta}]_{0:T})} \tag{2}$$

where $PL([\hat{F},\hat{\theta}]_{0:T})$ is the physics law used to restrict the hierarchical structure of the generated data, which provides the additional information to the regularize the learning process from the small sample data. In this case, we use the Lagrange equation of motion [37] as the physics law, which is defined as follows.

$$\begin{aligned} PL([\hat{F},\hat{\theta}]_{0:T}) = &\frac{1}{T}\sum_{t=1}^{T}(m(\hat{\theta}_t)\ddot{\hat{\theta}}_t + c(\hat{\theta}_t,\dot{\hat{\theta}}_t) \\ &+ g(\hat{\theta}_t) - \sum_{n=1}^{N} r_n \cdot \hat{F}_t^n)^2 \end{aligned} \tag{3}$$

where T is the number of time-steps, N is the channels of the $\hat{F}$, $m(\hat{\theta}_t)$, $c(\hat{\theta}_t,\dot{\hat{\theta}}_t)$, and $g(\hat{\theta}_t)$ denote mass matrix, the Centrifugal and Coriolis force, and the gravity, respectively [17] and r_n is the moment arm of the muscle $\hat{F}^n$, which is exported from OpenSim. In this manner, the G_σ will generate the structured outputs of $(\hat{F},\hat{\theta})$.

The $Q_{D(\phi)}^{G(\sigma)}$ is computed by the $D(\phi)$ and interprets the physics constraint action values as the estimated probability of being physics real by $D(\phi)$. These physics constraint action values lead to the improvement of GAN model in physical extrapolation from the small training data. The $Q_{D(\phi)}^{G(\sigma)}$ can be formulated as:

$$\begin{aligned} &Q_{D\phi}^{G\sigma}((G_\sigma(sEMG_{0:T}), [F,\theta]_{0:T}) = \\ &\mathbb{E}_{[\hat{F},\hat{\theta}]_{0:T}\sim[F,\theta]_{0:T}}[\log D\phi([\hat{F},\hat{\theta}]_{0:T})] + \\ &\mathbb{E}_{[\hat{F},\hat{\theta}]_{0:T}\sim G_\sigma(sEMG_{0:T}))}[\log(1 - D\phi([\hat{F},\hat{\theta}]_{0:T}))] \end{aligned} \tag{4}$$

For each epoch, once the new R_G and $Q_{D(\phi)}^{G(\sigma)}$ has been obtained, the policy model $G(\sigma)$ will be updated following the gradient of the reward function as follows.

$$\begin{aligned} \nabla_\sigma J(\sigma) = &\mathbb{E}_{[\hat{F},\hat{\theta}]_{0:T}\sim G_\sigma(sEMG_{0:T})} \\ &\sum \nabla_\sigma R_{G_\sigma}([\hat{F},\hat{\theta}]_{0:T} | [F,\theta]_{0:T}) \\ &\cdot Q_{D_\phi}^{G_\sigma}([\hat{F},\hat{\theta}]_{0:T}, [F,\theta]_{0:T}) \end{aligned} \tag{5}$$

Using likelihood ratios, the unbiased estimation for Eq. 5 on one epoch can be described as follows.

$$\begin{aligned} &\nabla_\sigma J(\sigma) \simeq \frac{1}{T}\sum_{t=1}^{T}\sum_{y_t\in[\hat{F},\hat{\theta}]_t} \nabla_\sigma R_{G_\sigma}(y_t | [F,\theta]_t) \\ &\cdot Q_{D_\phi}^{G_\sigma}(y_t, [F,\theta]_t) \\ &= \frac{1}{T}\sum_{t=1}^{T}\sum_{y_t\in[\hat{F},\hat{\theta}]_t} G_\sigma(y_t | [F,\theta]_t)\nabla_\sigma \log G_\sigma(y_t | [F,\theta]_t) \\ &\cdot Q_{D_\phi}^{G_\sigma}(y_t, [F,\theta]_t) \end{aligned} \tag{6}$$

The parameters of the policy model G_σ can be updated as follows.

$$\sigma \leftarrow \sigma + \alpha\nabla_\sigma J(\sigma) \tag{7}$$

where $\alpha \in \mathbb{R}$ is the learning rate.

Algorithm 1 Generative adversarial learning via physics-informed policy gradient

Require: generator network G_σ; discriminator D_ϕ; input multi-channel sEMG dataset $sEMG = \{X_{1:T}\}$; Inverse dynamics positive samples Pos

```
Initialize G_σ, D_φ with random weights σ, φ.
Pre-train G_σ using MLE on sEMG
Pos ← G_σ
Generate negative samples using G_σ for training D_φ
Pre-train D_φ via minimizing the cross entropy
repeat
  for G_σ training-steps do
    Generate [F̂, θ̂] time series via G_σ
    for t in 0:T do
      Compute Q^{Gσ}_{Dφ} by Eq. 4
    end for
    Update generator parameters via physics-informed
    reward Eq. 7
  end for
  for d-steps do
    Use current G_σ to generate negative examples and
    combine them with given positive examples Pos
    Train discriminator D_φ for k epochs.
  end for
  β ← σ
until GAN converges
```

To summarize, Algorithm 1 provides an in-depth look at our proposed GAN optimization via a physics-informed policy gradient. Initially, G_σ is pre-trained on the training set $sEMG = \{X_{1:T}\}$ using the maximum likelihood estimation (MLE). And then, the G_σ and D_ϕ undergo adversarial learning. As the G_σ improves, the D_ϕ is routinely retrained to stay synchronized with the G_σ improvement. We ensure balance by generating an equal number of negative samples for each training step as the positive samples.

This article has been accepted for publication in IEEE Journal of Biomedical and Health Informatics. This is the author's version which has not been fully edited and content may change prior to final publication. Citation information: DOI 10.1109/JBHI.2023.3347672

B. The generative network

The proposed physics-informed low-shot learning method does not depend on the specific generative network architecture. In this study, considering the long-term temporal dependencies of the F and θ sequences to the input multi-channel sEMG sequence, we employ the Long Short-Term Memory (LSTM) cells to our generative model [39]. The architecture of the generator network G is shown in Fig.2. It serves three functions: multi-channel sEMG feature extraction, residual learning with LSTM, and musculoskeletal tokens sequence generation.

Firstly, for the multi-channel sEMG feature extraction, a 1-dimensional (1D) convolution filter with a $2/times1$ kernel is introduced to capture the multiple sEMG features at time step t. The extracted convolution features represent the hierarchical structures of the multi-channel sEMG. In this study, the convolution kernel is set to $1 \times b$ for a b-channel sEMG input. Considering the batch normalization (BN) layer would normalize the features and get rid of the range flexibility for upscaling features [40], no BN layer is used here to avoid blurring the sEMG responses hidden in the extracted features. The max-pooling layer is used to combine the extracted sEMG features into a single neuron by using the maximum value from each convolution window. The max-pooling operation reduces the number of parameters and network computation costs and has the effect of adjusting over-fitting.

Secondly, the LSTM blocks are employed for residual learning of the time-series characteristics of the target musculoskeletal tokens. The LSTM layer is well suited for time-series sequence generation by addressing the explosive and vanishing gradient issues [38]. An LSTM block consists of a memory cell, an input gate, an output gate, and a forget gate, the detailed definitions of the components are described in [40]'s study. Specifically, in this study, in time step t, the memory cell remembers structured feature values over the previous $t-1$ intervals and the three gates regulate the flow of information into and out of the memory cell, which has a great preference for preserving long-term temporal structure characteristics by consolidating previous temporal correlations as memory units. Meanwhile, the high-level sEMG features extracted from the convolution layer represent the current multi-channel sEMG responses to muscle force and joint kinematics. The skip-connect of the memory cell and the high-level sEMG features not only represent extracted local kinetic invariances but also represent the temporal dynamics of the motions.

It is noteworthy that the traditional LSTM layer only produces fitness between the current time step and the previous time steps. However, we expect the model also can pay insight into the resulting future outputs. In order to compute the action value for future physical fitness, a Monte Carlo (MC) search with a roll-out strategy is used to sample the unknown last $T-t$ time steps. and the N-time Monte Carlo search can be formulated as:

$$\{(F_{0:T}, \theta_{0:T})^1, ..., (F_{0:T}, \theta_{0:T})^N = MC(F_{0:t}, \theta_{0:t})\} \tag{8}$$

Finally, the output of the LSTM unit is flattened to a feature vector and the fully connected layers are used to decode the high-level features into the muscle force F and joint kinematics θ sequence over a motion period.

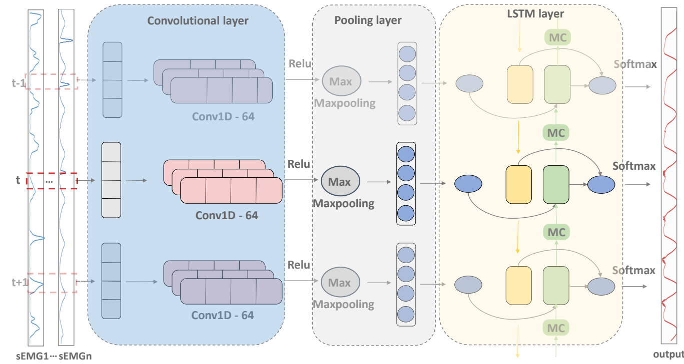

Fig. 2. The network architecture of the generator network in the proposed physics-informed reinforcement generative adversarial learning.

C. The discriminative model

In this study, a ϕ parameterized discriminator network D_ϕ is built to guide the iterations of G_σ from the small sample data. D_ϕ outputs a probability indicating the heterogeneity between $[\hat{F}, \hat{\theta}]$ and $[F, \theta]$. For this purpose, we employ a convolution neural network (CNN) [41] as the discriminative model because of its successful applications in sequence classification. In this study, we concentrate on the situation where the discriminator estimates the likelihood of a completed $[\hat{F}, \hat{\theta}]$ time-series from the physical-law model (i.e. ID).

We first represent an input muscle force and joint kinematics time series $x_1, ..., x_T$ as

$$E_{0:T} = [\hat{F}, \hat{\theta}]_0 \oplus [\hat{F}, \hat{\theta}]_2 \oplus ... \oplus [\hat{F}, \hat{\theta}]_T \tag{9}$$

where, $x_t \in \mathbb{R}^b$ is the muscle force and joint kinematics in time-step t and $\oplus$ is the concatenation operator to build the matrix $E_{1:T} \in \mathbb{R}^T$. Then the convolution operator is used to produce a new feature map:

$$c_i = \rho(w \odot E_{i:i+l-1} + b) \tag{10}$$

where $\odot$ is the element-wise production, b is a bias term and ρ is a non-linear function. In this study, the discriminator, as shown in Fig.3, employs various numbers of kernels with different window sizes to extract different features from the input musculoskeletal sequence. And the max-pooling operation over the feature maps to reduce the number of parameters and network computation costs. In order to enhance the discrimination performance, a highway operator [42] based on the pooled feature maps is also employed in our discriminative model. Finally, a fully connected layer with softmax activation is used to output the estimation of the likelihood that the input sequence conforms to physical laws.

III. MATERIAL AND EXPERIMENTAL METHODS

In this study, we test our proposed method on two joint motion scenarios. The first one is the knee joint modeling

This article has been accepted for publication in IEEE Journal of Biomedical and Health Informatics. This is the author's version which has not been fully edited and content may change prior to final publication. Citation information: DOI 10.1109/JBHI.2023.3347672

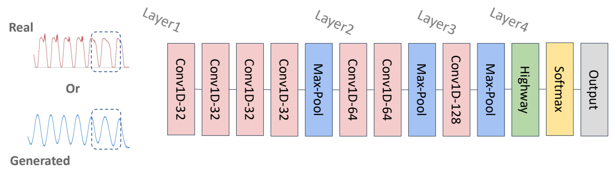

Fig. 3. The network architecture of the discriminative model in the proposed physics-informed reinforcement generative adversarial learning.

from an open-access dataset of walking trials, and the second one is the wrist joint modeling from the self-collected dataset of wrist motions.

A. Open-access dataset of walking trials

The open-access dataset of walking trails is obtained from a real-world experiment reported in [43]. This dataset involves six healthy participants with an average age of 12.9 $\pm$ 3.2 years and an average weight of 51.8 $\pm$ 19.1 Kg. Participants are instructed to walk at four distinct speeds, which include very slow (0.53 $\pm$ 0.1 m/s), slow (0.75 $\pm$ 0.1 m/s), free (1.15 $\pm$ 0.08 m/s), and fast (1.56 $\pm$ 0.21 m/s) speeds. The sEMG signals are captured from the $bicepsfemorisshorthead$ (BFS) and the $rectusfemoris$ (RF) as they are the primary flexor and extensor of the knee joint. In this study, we normalize each gait cycle into 100 frames for model training and testing, and the original data for model extrapolation evaluation. In the model training and testing session, each walking trial sample is formatted into a source matrix that includes the time step, gait motion data (i.e. ground truth θ and the inverse dynamics-based F), and enveloped sEMG signals. All of the samples from different participants are combined to create a comprehensive dataset for model training and testing.

B. Self-collected dataset of wrist motions

Our wrist motions experiment, approved by the MaPS and Engineering Joint Faculty Research Ethics Committee of the University of Leeds (MEEC 18-002), involved six participants with signed consent. Participants were instructed to keep their torso straight with their shoulder abducted at 90 degrees and their elbow joint flexed at 90 degrees. The VICON motion capture system is used to record continuous wrist flexion/extension motion. Joint motions are calculated using an upper limb model with 16 reflective markers with 250 Hz sampling rate. Concurrently, sEMG signals are captured from the primary wrist muscles (n = 1, 2,..., 5), including the $flexorcarpiradialis$ (FCR), the $flexorcarpiulnaris$ (FCU), the $extensorcarpiradialislongus$ (ECRL), the $extensorcarpiradialisbrevis$ (ECRB), and the $extensorcarpiulnaris$ (ECU) using Avanti Sensors (sampling rate is 2000 Hz). Electrodes are placed by palpation and their placement is validated by observing the signal during contraction before the experiment. The sEMG signals and motion data (i.e. ground truth θ and the inverse dynamics-based F) were synchronized and resampled at 1000 Hz. Each participant performed five repetitive trials with a three-minute break between trials to prevent muscle fatigue.

Fig. 4. Experimental picture for sEMG collection: electrodes are placed on five primary muscles of wrist joint, including FCR, FCU, ECU, ECRL and ECRB. More experimental details can be found in [44]

The recorded sEMG signals are pre-processed by a 20 Hz and 450 Hz band-pass filter, full rectification, and a 6 Hz low-pass filter. These signals are then normalized based on the maximum voluntary contraction recorded prior to the experiment, yielding the enveloped sEMG signals. The reason for using the envelopes sEMG is that, compared with the raw sEMG signals, the enveloped sEMG, being smoother, might lead to more stable generator training as they reduce high-frequency noise and fluctuations present in the raw signals, and further alleviate the problems during the learning process, such as training stability, convergence speed, feature representation, and overfitting. We normalize each motion cycle into 156 frames for model training and testing, and the original data for model extrapolation evaluation. A total of 360 motion data are then combined to create a comprehensive dataset for model training and testing, and 6 motion data are used for model evaluation.

C. Benchmark models and parameter settings

To evaluate the performance and effectiveness of the proposed physics-informed policy gradient for low-shot generative adversarial learning, the benchmark models employ three representative methods, including physics-Informed convolutional neural network (PI-CNN) [17] which represents the state-of-the-art deep learning based musculoskeletal modeling method, ML-ELM [45] which represents the general musculoskeletal modeling method, and the vanilla GAN which represents the traditional GAN family without physical-law [32].

D. Evaluation metrics

The evaluation metrics include 1) the metrics for evaluating the quality of the generated samples including the information entropy associated peak signal-to-noise ratio (PSNR) [46], coefficient of Determination (R^2) [47], root mean square error (RMSE) [18], Spearman's Rank Correlation Coefficient

(SRCC) [48], and 2) the metrics for evaluating the mode collapse of GANs, including 1) inception score (IS) [34], and 2) Frechet inception distance (FID) [49].

The IS measures both the quality of generated time-series data and their diversity, reflecting the probability of mode collapse in the model training process. In this study, we refer thereferenced $[\hat{F}, \hat{\theta}]$ as ref and the generated data $G_\sigma(sEMG_{0:T})$ as g. It is desirable for the conditional probability, $p(ref|g)_{0:T}$ to be highly predictable (low entropy), that is, the probability density function is less uniform. The diversity of the generated data can be measured with the marginal probability, $p(ref_{0:T}) = \int p(ref|g)$. The less uniform (low entropy) the marginal probability is, the less the diversity of the generated data is. Through computing the KL-divergence between these two probability distributions, the IS is computed with the equation below:

$$IS = exp[\mathbb{E}_{sEMG \sim p(sEMG)}[\mathbb{D}_{KL}(p(ref|g)||ref)]] \quad (11)$$

The Frechet Inception Distance (FID) score is a metric calculating the distance between the feature vectors extracted from the reference and generated data. The FID is sensitive to mode collapse. Through modelling the distribution of the features extracted from an intermediate layer with a multivariate Gaussian distribution, the FID between the reference and generated data is calculated using the following equation.

$$FID = ||M_{ref} - M_g||_2^2 + Tr(C_{ref} + C_g - 2(C_{rf} \times C_g)^{1/2}) \quad (12)$$

where M_{rf} and M_g refer to the feature-wise means of the referenced $[\hat{F}, \hat{\theta}]$ and the generated data $G_\sigma(sEMG_{0:T})$ in discriminator model, respectively, and C_{ref} and C_g are the covariance matrix for the referenced and generated feature vectors, respectively.

IV. Results and Discussion

In this section, we evaluate the performance of the proposed physics-informed low-shot learning in the knee joint and wrist joint scenarios. We first carry out overall comparisons of the results from the proposed and benchmark methods. We also evaluate the model performance on small training data and handling mode collapse. Lastly, we investigate the robustness and generalization performance of the proposed method in intersession scenarios. The training of the proposed framework and benchmark methods was conducted using PyTorch on a workstation equipped with NVIDIA Quadro K4200 graphics cards and 256G RAM.

A. Overall evaluation of the muscle force dynamics modeling

In this section, we first carry out overall comparisons between the proposed and benchmark methods on the test dataset. Fig. 5 demonstrates the overall results of the joint kinematics generation in one motion circle from the proposed and benchmark methods for both the knee joint (the first row of Fig. 5) and wrist joint cases (the second row of Fig. 5). The average joint kinematics and standard deviation distribution from the proposed method align well with the ground truth

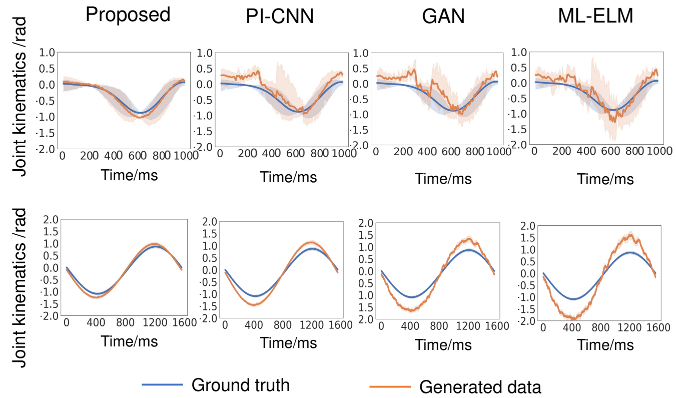

Fig. 5. Comparison of the average knee joint kinematics (the first row) and wrist joint kinematics (the second row) within one motion cycle between the ground truth and the generated data from the proposed and benchmark models. The shaded areas represent the mean $\pm$ one standard deviation of the kinematics.

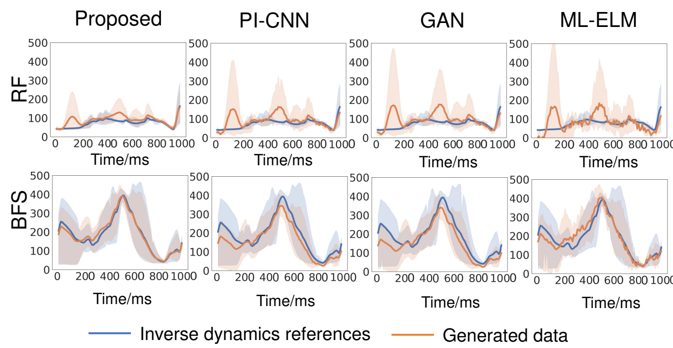

Fig. 6. Comparison of the average knee muscle force dynamics within one gait cycle between the real-target and the generated muscle force data from the proposed and benchmark models. The shaded areas represent the mean $\pm$ one standard deviation of the muscle force for BFS and RF.

in both the knee joint and wrist joint cases. These findings indicate the proposed model achieves the best performance among the benchmark models on the unbiased estimation of the joint kinematics.

Similarly, Fig. 6 and Fig.7 demonstrates the overall results of the muscle force estimations in one motion circle for both the knee joint (i.e. RF and BFS) and wrist joint (i.e. FCR, FCU, ECRL, ECRB, and ECU) cases, respectively. The average muscle forces estimated by the proposed method align well with the inverse dynamics, demonstrating the excellent multiple muscle tracking capability of the proposed model. In addition, the standard deviation distribution of the proposed model-generated muscle forces is perfectly consistent with the standard deviation distribution of the inverse dynamics-based references. More importantly, the muscle force estimated by the proposed method is more sensitive to the biophysical fluctuations of the referenced muscle force. These results indicate that the proposed model achieves the best performance among the benchmark models on the unbiased estimation of the muscle force from the multi-channel sEMG signals.

To further assess the extrapolation performance quantita-

This article has been accepted for publication in IEEE Journal of Biomedical and Health Informatics. This is the author's version which has not been fully edited and content may change prior to final publication. Citation information: DOI 10.1109/JBHI.2023.3347672

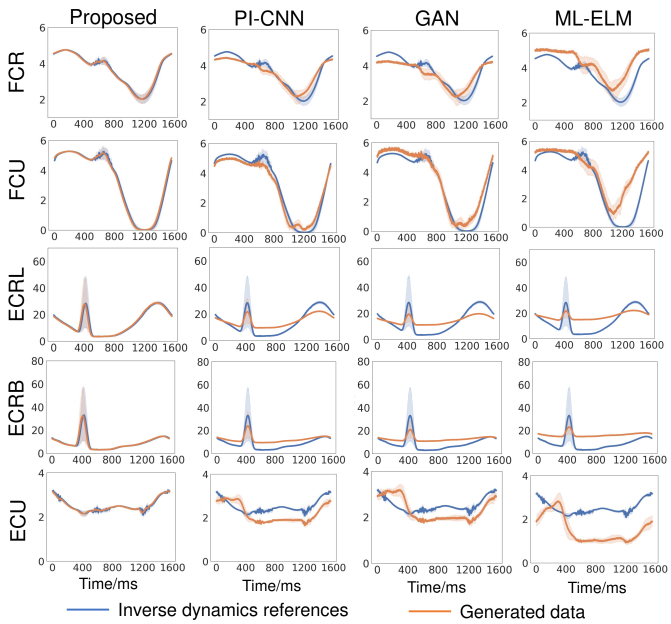

Fig. 7. Comparison of the average wrist muscle force dynamics within one motion cycle between the real-target and the generated muscle force data from 5-channel sEMG signal. The shaded areas represent the mean ± one standard deviation of the muscle force for FCR, FCU, ECRL, ECRB, and ECU.

tively, we present detailed comparisons of the proposed and benchmark models on both the test data and evaluation data. Table I and Table II respectively show the results for the knee joint case and the wrist joint case. The results indicate that the proposed model performs best on both of the testing and evaluation data. Specifically, for model testing, the $PSNR$, R^2, $RMSE$, $SRCC$ of the proposed model are 15.57%, 6.22%, 28.08%, 7.2% higher than that of the second best model (i.e. PI-CNN). For model evaluation, the $PSNR$, R^2, $RMSE$, $SRCC$ of the proposed model are 24.72%, 16.29%, 38.99%, 17.66% higher than that of the second best model (i.e. GAN). In addition, because the evaluation data involve the original sEMG recordings, the comparison of the testing results and evaluation results indicates the model extrapolation from the experimental scenarios to real scenarios. The proposed model shows the best-extrapolated estimation of muscle force and joint kinematics among the benchmark models, the results from the testing data and evaluation data are consistent. In contrast, the performance of the benchmark models shows a serious decline in evaluation data.

B. Evaluation of real-time performance

The real-time performance metrics, including the long-term accuracy, inference latency, and model throughput, are important to evaluate the model performance in real-world scenarios with varied locomotion amplitudes and periods. In this section, we use joint kinematics estimation as a study case to evaluate the real-time performance of our proposed models. Firstly, to evaluate the long-term accuracy, the proposed model and the benchmark models are performed on the original joint kinematics (ground truth) data. The comparisons, as shown in Fig. 8, illustrate that the proposed model performs best

TABLE I
THE EVALUATION OF THE PROPOSED AND BENCHMARK MODELS ON KNEE JOINT CASE WITH TWO-CHANNELS sEMG.

	Methods	PSNR	R^2	RMSE	SRCC
		Model test			
RF	Proposed	91.91	0.88	11.32	0.92
	PI-CNN	77.45	0.84	19.64	0.85
	GAN	75.54	0.82	18.25	0.81
	ML-ELM	59.94	0.76	25.62	0.72
BFS	Proposed	93.45	0.93	11.93	0.93
	PI-CNN	76.93	0.87	19.21	0.83
	GAN	76.17	0.85	18.35	0.79
	ML-ELM	62.66	0.78	26.43	0.73
θ	Proposed	34.79	0.91	5.73	0.92
	PI-CNN	30.16	0.84	5.97	0.89
	GAN	30.89	0.88	6.57	0.85
	ML-ELM	21.33	0.75	11.25	0.73
		Model evaluation			
RF	Proposed	88.89	0.82	11.21	0.83
	PI-CNN	58.91	0.59	24.17	0.6
	GAN	68.72	0.7	26.51	0.69
	ML-ELM	46.79	0.53	28.75	0.5
BFS	Proposed	91.84	0.91	11.91	0.84
	PI-CNN	58.19	0.61	23.58	0.58
	GAN	69.26	0.72	25.79	0.67
	ML-ELM	49.21	0.55	38.98	0.51
θ	Proposed	34.89	0.92	5.45	0.91
	PI-CNN	23.43	0.59	8.3	0.62
	GAN	28.27	0.75	7.89	0.72
	ML-ELM	17.19	0.53	18.44	0.51

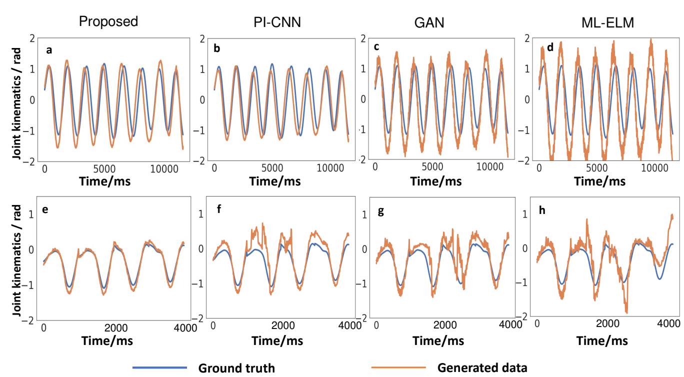

Fig. 8. Comparison of the real-time performance of the proposed model and the benchmark models on long-term joint kinematics estimation for wrist joint case (a-d) and knee joint case (e-f).

accuracy for the long-time joint kinematics estimation on both the wrist joint and knee joint cases. In contrast, the benchmark models (e.g. see Fig. 8f-h) do not fit well with the varied amplitudes of the real-time joint kinematics dynamics. Such findings are consistent with the results investigated in section IV-A, suggesting that the proposed model achieves the most robust results on real-time joint kinematics estimations.

Secondly, to evaluate the balance of the models between the inference latency and model throughput, we conduct the comparison of the inference latency and model throughput of the proposed model and the benchmark models for the real-time long-term joint kinematics estimation, as shown in Fig. 9. Our results show that, while PI-CNN has the lowest latency

This article has been accepted for publication in IEEE Journal of Biomedical and Health Informatics. This is the author's version which has not been fully edited and content may change prior to final publication. Citation information: DOI 10.1109/JBHI.2023.3347672

TABLE II
THE EVALUATION OF THE PROPOSED AND BENCHMARK MODELS ON WRIST JOINT CASE WITH FIVE-CHANNELS SEMG

	Methods	PSNR	R^2	RMSE	SRCC		Methods	PSNR	R^2	RMSE	SRCC
Model test											
FCR	Proposed	31.91	0.92	5.32	0.94	FCU	Proposed	33.61	0.93	4.37	0.96
	PI-CNN	27.45	0.84	9.64	0.83		PI-CNN	29.01	0.86	10.43	0.83
	GAN	25.54	0.86	8.25	0.81		GAN	25.27	0.88	8.6	0.79
	ML-ELM	19.94	0.74	15.62	0.72		ML-ELM	18.42	0.76	14.95	0.73
ECRL	Proposed	84.21	0.95	14.68	0.94	ECRB	Proposed	82.93	0.95	14.78	0.97
	PI-CNN	79.4	0.84	25.08	0.83		PI-CNN	79.75	0.88	24.32	0.81
	GAN	61.54	0.9	24.55	0.82		GAN	59.71	0.91	24.62	0.79
	ML-ELM	57.76	0.77	42.41	0.76		ML-ELM	57.4	0.78	41.82	0.77
ECU	Proposed	30.81	0.92	5.14	0.92	θ	Proposed	34.32	0.97	3.75	0.96
	PI-CNN	30.31	0.84	10.06	0.82		PI-CNN	29.94	0.84	4.63	0.88
	GAN	28.06	0.87	7.92	0.8		GAN	30.34	0.86	4.51	0.85
	ML-ELM	19.85	0.75	14.72	0.71		ML-ELM	21.15	0.76	9.62	0.74
Model evaluation											
FCR	Proposed	29.96	0.87	5.05	0.89	FCU	Proposed	31.35	0.88	4.15	0.91
	PI-CNN	20.49	0.63	10.23	0.62		PI-CNN	21.75	0.65	9.82	0.62
	GAN	22.43	0.77	11.43	0.73		GAN	21.8	0.79	12.74	0.71
	ML-ELM	14.09	0.56	19.72	0.54		ML-ELM	13.57	0.57	21.21	0.55
ECRL	Proposed	79.76	0.9	13.95	0.89	ECRB	Proposed	78.33	0.9	14.04	0.92
	PI-CNN	58.65	0.63	28.81	0.62		PI-CNN	59.81	0.66	28.24	0.61
	GAN	54.52	0.81	32.1	0.74		GAN	53.7	0.82	24.11	0.71
	ML-ELM	42.45	0.58	39.81	0.57		ML-ELM	42.3	0.59	51.37	0.58
ECU	Proposed	28.64	0.87	4.88	0.87	θ	Proposed	31.75	0.92	3.56	0.91
	PI-CNN	22.29	0.63	10.55	0.62		PI-CNN	21.73	0.63	6.47	0.66
	GAN	24.41	0.78	11.13	0.72		GAN	25.58	0.77	8.06	0.77
	ML-ELM	14.28	0.56	16.04	0.53		ML-ELM	15.43	0.57	11.22	0.56

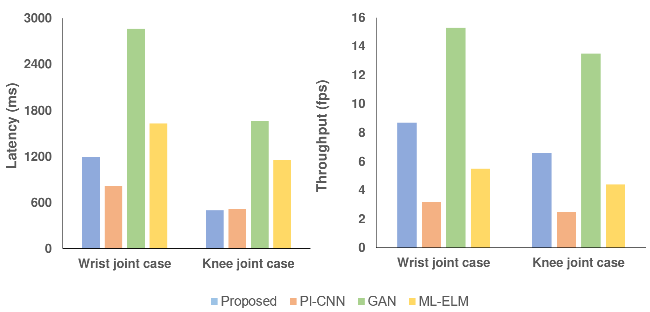

Fig. 9. The inference latency and model throughput of the proposed model and the benchmark models for the real-time evaluations .

time and GAN has the highest throughput, the proposed model achieves a great balance between inference latency and model throughput (i.e. it achieves the second-best real-time performance on both the latency time and throughput evaluation). These resultant findings suggest that the proposed model achieves the best real-time performance on the long-term estimation of the joint kinematics estimations.

C. Evaluation of low-shot learning

The proposed physics-informed policy gradient incorporates the temporal relationship of the muscle force and joint kinematics dynamics from the Lagrange motion equation, resulting in an improved kinetics estimation from the low-shot samples. Initially, the physical information is used to constrain the model reward accumulated following the periodic multi-channel sEMG signals. And then, the accumulative reward is used to guide the Monte Carlo search to generate the unbiased estimation of muscle force and joint kinematics dynamics.

To quantitatively assess the effectiveness of the proposed method on low-shot learning, we firstly regard the modeling results shown in Table I and Table II as the baselines that represent the optimal performance of the proposed and benchmark models, and then we train the models with different training sample sizes for 1500 epochs as low-shot learning learning. The percentages of the low-shot learning learning results and the baseline joint kinematics modeling results, denote as $P-PSNR$, $P-R^2$, $P-RMSE$, and $P-SRCC$, are used as the evaluation metrics to describe what percentage of the performance of the baseline models can be achieved with the new models.

The evaluation of the low-shot learning of the proposed and benchmark models on the knee joint and wrist joint kinematics modeling is shown in Table III. It is obvious that the proposed model with a physics-informed policy gradient outperforms all of the benchmark models in low-shot learning. The 10-shot learning is able to achieve over 80% baseline performance in terms of $PSNR$, R^2, $RMSE$, and $SRCC$. In comparison, the PI-CNN and GAN models require at least 80-shot learning to reach the similar modeling performance. Therefore, it can be inferred that the proposed physics-informed policy gradient relies heavily on the physical representations and temporal structural characteristics of the training data, rather than the quantity of the data. This is encouraging as it suggests that the proposed method facilitates the applications of deep learning in biomechanical engineering from the general issue of limited sample size.

D. Mode collapse evaluation

Mathematically, the generative model is easy to find a biased estimation caused by mode collapse, which leads to the generated samples only being located in the partial real

This article has been accepted for publication in IEEE Journal of Biomedical and Health Informatics. This is the author's version which has not been fully edited and content may change prior to final publication. Citation information: DOI 10.1109/JBHI.2023.3347672

TABLE III
EVALUATION OF THE LOW-SHOT LEARNING PERFORMANCE OF THE PROPOSED AND BENCHMARK MODELS ON JOINT KINEMATICS MODELING. THE $P-PSNR$, $P-R^2$, $P-RMSE$, AND $P-SRCC$ RESPECTIVELY REPRESENT THE SNR, R^2, $RMSE$, AND $SRCC$ OF THE n-SHOT LEARNING AS A PERCENTAGE OF THE VALIDATION METRICS OF THE BEST JOINT KINEMATICS RESULTS REPORT IN TABLE.I AND TABLE II.

		Knee joint case				Wrist joint case			
		P-PNSR	P-R^2	P-RMSE	P-SRCC	P-PNSR	P-R^2	P-RMSE	P-SRCC
Proposed	1-shot	75%	74%	76%	75%	76%	73%	77%	75%
	10-shot	83%	82%	84%	87%	82%	81%	84%	88%
	20-shot	86%	84%	86%	86%	87%	86%	88%	84%
	40-shot	92%	91%	92%	91%	93%	91%	93%	94%
	60-shot	94%	94%	92%	94%	96%	97%	93%	93%
	80-shot	93%	94%	95%	94%	92%	93%	97%	94%
	100-shot	95%	94%	93%	93%	96%	94%	93%	96%
		P-PNSR	P-R^2	P-RMSE	P-SRCC	P-PNSR	P-R^2	P-RMSE	P-SRCC
PINN	1-shot	41%	41%	41%	39%	42%	42%	44%	39%
	10-shot	44%	42%	44%	44%	46%	42%	45%	47%
	20-shot	68%	69%	72%	73%	69%	70%	72%	76%
	40-shot	76%	76%	77%	79%	77%	78%	8%	78%
	60-shot	79%	77%	76%	75%	78%	77%	76%	76%
	80-shot	82%	83%	84%	85%	81%	86%	83%	84%
	100-shot	84%	87%	85%	87%	85%	88%	85%	86%
		P-PNSR	P-R^2	P-RMSE	P-SRCC	P-PNSR	P-R^2	P-RMSE	P-SRCC
GAN	1-shot	46%	44%	47%	49%	45%	45%	48%	51%
	10-shot	45%	45%	45%	47%	48%	46%	44%	48%
	20-shot	66%	69%	7%	73%	67%	71%	70%	73%
	40-shot	72%	73%	74%	74%	74%	72%	72%	76%
	60-shot	79%	78%	81%	81%	78%	78%	80%	8%
	80-shot	81%	83%	85%	85%	79%	83%	86%	84%
	100-shot	84%	86%	87%	89%	86%	87%	86%	91%
		P-PNSR	P-R^2	P-RMSE	P-SRCC	P-PNSR	P-R^2	P-RMSE	P-SRCC
ML-ELM	1-shot	36%	35%	37%	38%	34%	37%	36%	37%
	10-shot	38%	44%	45%	39%	39%	39%	42%	38%
	20-shot	57%	56%	55%	54%	59%	56%	57%	55%
	40-shot	62%	62%	65%	59%	65%	61%	68%	58%
	60-shot	66%	65%	67%	66%	65%	64%	66%	67%
	80-shot	75%	73%	72%	74%	77%	74%	71%	74%
	100-shot	78%	79%	78%	81%	78%	82%	81%	82%

distribution where it can fool the discriminative model and ignore other modes of real distribution during the adversarial learning. To handle this issue, the proposed physics-informed policy gradient alleviates the random noises and makes the generated feature sequence governed by the physics law, which facilitates the estimation of compound kinematics patterns and achieves the unbiased estimation of kinematics generation.

In order to evaluate the performance of the proposed method on alleviating the mode collapse, we test and compare the proposed model with the benchmark model from two aspects: 1) a quantitative evaluation of the diversity of the generated motions, based on the distance-derived IS and FID metrics; and 2) a monotonicity assessment on the generator iterations during the network training process.

Firstly, the quantitative evaluation for the diversity of the generated motions is conducted on the testing dataset. The higher IS and lower FID indicate the better diversity of the generated motion samples, which further indicates the alleviation of mode collapse. The results demonstrated in Table IV show the proposed model outperforms the competitors in terms of the IS and FID measurements for both the knee joint and wrist joint motion generation. In addition, the benchmark GAN model, with the network architecture as same as the proposed model, is 32.83% lower in IS, and 14.1% higher in FID than the proposed model. These findings suggest that the proposed physics-informed policy gradient optimization approach has great performance in alleviating the mode collapse during adversarial learning.

TABLE IV
THE COMPARISON OF INCEPTION SCORES (IS) AND FRECHET INCEPTION DISTANCES (FID) OF THE JOINT KINEMATICS GENERATED FROM THE PROPOSED AND BENCHMARK MODELS ON THE MODEL TEST DATASETS.

	Knee joint case		Wrist joint case	
	IS	FID	IS	FID
Proposed	15.39	64.22	12.5	41.95
PINN	12.68	71.13	8.03	48.8
GAN	13.11	78.54	8.43	46.13
ML-ELM	10.59	79.83	6.79	57.05

Secondly, in order to further explore the performance of the proposed physics-informed policy gradient on the mode collapse issue, we compare the generator iterations of the same GAN architectures with and without the physics-informed policy gradient (Fig. 10). Because we trained our model on

This article has been accepted for publication in IEEE Journal of Biomedical and Health Informatics. This is the author's version which has not been fully edited and content may change prior to final publication. Citation information: DOI 10.1109/JBHI.2023.3347672

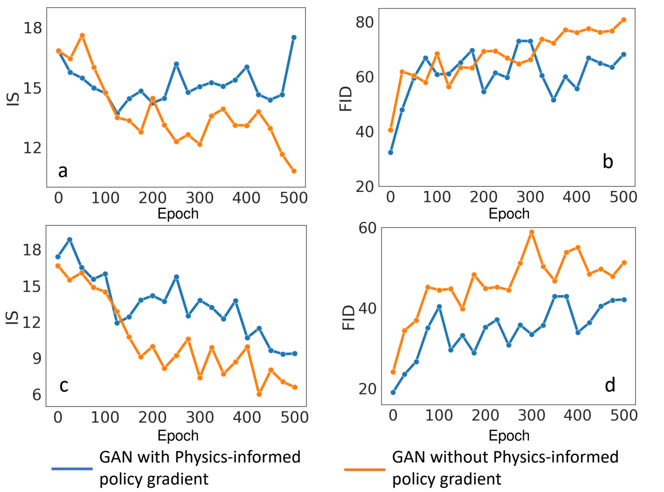

Fig. 10. Changes of IS and FID scores of the generated joint kinematics during the first 500 iterations of the GAN model using the proposed physics-informed policy gradient and the typical GAN without using the physics-informed policy gradient. The test is conducted on knee joint cases (a) and (b) and wrist joint cases (c) and (d), respectively.

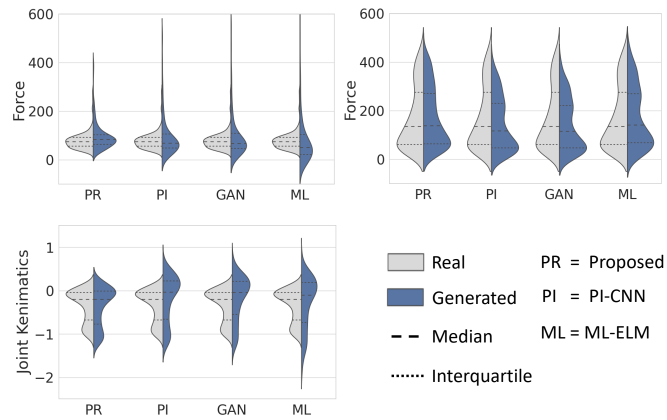

Fig. 11. Robustness evaluation of the proposed model (PR), PI-CNN (PI), GAN, and ML-ELM (ML) on the intra-session scenario.

a few-shot dataset, the training data only covered limited variations and modes. Therefore, in the initial stage of training, the generator will generate data with more discrete diversities (similar to random noise) than the reference. As training progressed and the model's accuracy improved, the variation in the data created by the generator began to mirror the reference data's distribution more closely. In the late stage of training, for the traditional GAN-based model, the diversity of the generated data may plateau or decrease due to the limitations of few-shot training and the occurrence of mode collapse. In contrast, our model, by introducing the proposed physics-informed policy gradient, is able to generate data following the physics law, which greatly enriches the diversity of generated samples for the few-shot reference samples. In addition, the IS and FID curves from the GAN with the proposed physics-informed policy gradient are more monotonous than the GAN without the physics-informed policy gradient, along with the increase of iteration number. Thus, the curves of IS from the proposed physics-informed policy gradient steadily increase and the curves of FID steadily decrease for both knee joint (10a and b) and wrist joint (10c and d) cases.

E. Model application on intra-session scenario

In musculoskeletal modeling, the intra-session scenario is regarded as the multiple sets of motions that occur within the same session. To test the robustness of the proposed model in the intra-session scenario, we use the knee joint data with different walking speeds for one subject as the intra-session evaluation dataset. The muscle force and joint kinematics modeling results, as shown in Fig. 11, indicate that the proposed framework performs best among the baseline methods. Importantly, the median and interquartile values of the proposed model with physics-informed policy gradient remain consistent with the real data across different walking speeds. In comparison, the median and quartiles of the baseline methods, such as the GAN model without using the physics-informed policy gradient, show significant inconsistencies with the real data, indicating a declined performance in the intra-session scenario due to the variability in walking speeds. These findings suggest that the model optimized by the proposed physics-informed policy gradient has great robustness in intra-session scenarios.

F. Model application on inter-session scenario

The inter-session scenario generally refers to a situation where motion data are collected across multiple sessions. To test the robustness of the proposed model in the inter-session scenario, we use the wrist joint data with different subjects as the evaluation dataset. The muscle force and joint kinematics modeling results, as shown in Fig. 12, indicate that the proposed framework performs best on the musculoskeletal modeling among the baseline methods. Specifically, the median and interquartile values of the proposed model with physics-informed policy gradient remain consistent with the real data across different subjects. In comparison, the baseline methods, such as the GAN model without using the physics-informed policy gradient, show a declined performance in the inter-session scenario due to the variability in walking speeds. These findings suggest that the model optimized by the proposed physics-informed policy gradient has great robustness in inter-session scenarios.

V. Conclusion

This paper develops a physics-informed low-shot adversarial learning method, which seamlessly integrates the Lagrange equation of motion and inverse dynamic muscle model into the GAN framework, for the unbiased estimation of the muscle force and joint kinematics from the small size sEMG time series. Specifically, the Lagrange equation of motion is introduced as physical constraint, which facilitates the generator to estimate the muscle force and joint kinematics with more temporal structural representations. Meanwhile, the physics-informed policy gradient rewards the physical consistency of the generated muscle force and joint kinematics and the inverse

This article has been accepted for publication in IEEE Journal of Biomedical and Health Informatics. This is the author's version which has not been fully edited and content may change prior to final publication. Citation information: DOI 10.1109/JBHI.2023.3347672

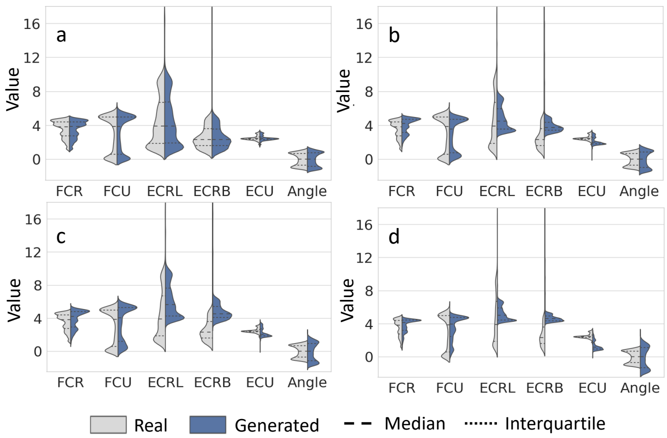

Fig. 12. Robustness evaluation of the a) proposed model, b) PI-CNN, c) GAN, and d) ML-ELM (ML) on the inter-session scenario.

dynamics-based references, which improve the extrapolation performance of the generative network. Comprehensive experiments on the knee joints and wrist joints indicate the feasibility of the proposed method. The resultant findings suggest that the proposed method performs well in handling the mode collapse issue of GAN on the small sample data, and the estimations of the muscle forces and joint kinematics are unbiased compared to the physics-based inverse dynamics. These findings suggest that the proposed method may reduce the gaps between laboratory prototypes and clinical applications. However, it is worth noting that the physics reference (i.e. the inverse dynamics for this study) plays an important role in constraining the physics representation of the generated samples. Therefore, the choice of physics module may vary when the proposed approach is extended to other application cases.

Going forward, we plan to delve deeper into the properties of the physics-informed deep learning framework in the context of sEMG-based musculoskeletal modeling. We aim to investigate the potential of the low-shot learning-based model on the continuous and simultaneous estimation of multiple joint kinematic chains from sEMG signals. For coupled joint movement, each joint can be represented as a generalized coordinate, and its interactions with other joints would result in coupled differential equations that describe the system's motion. And then we can use the coupled motion equations to replace the physics law we used in Eq.3 to guide the model training for coupled joint movement. We also plan to adjust the compositions of the proposed method to cater to different application scenarios. Furthermore, we intend to evaluate the reliability and accuracy of the proposed framework through coupled joint movement.

References

[1] A. Falisse, G. Serrancolí, C. L. Dembia, J. Gillis, I. Jonkers, and F. De Groote, "Rapid predictive simulations with complex musculoskeletal models suggest that diverse healthy and pathological human gaits can emerge from similar control strategies," *Journal of The Royal Society Interface*, vol. 16, no. 157, p. 20190402, 2019.

[2] L. Modenese and J. Kohout, "Automated generation of three-dimensional complex muscle geometries for use in personalised musculoskeletal models," *Annals of Biomedical Engineering*, vol. 48, no. 6, pp. 1793–1804, 2020.

[3] S. H. Smith, R. J. Coppack, A. J. van den Bogert, A. N. Bennett, and A. M. Bull, "Review of musculoskeletal modelling in a clinical setting: Current use in rehabilitation design, surgical decision making and healthcare interventions," *Clinical Biomechanics*, vol. 83, p. 105292, 2021.

[4] A. Kotsifaki, S. Van Rossom, R. Whiteley, V. Korakakis, R. Bahr, V. Sideris, and I. Jonkers, "Single leg vertical jump performance identifies knee function deficits at return to sport after acl reconstruction in male athletes," *British journal of sports medicine*, vol. 56, no. 9, pp. 490–498, 2022.

[5] D. J. Braun, V. Chalvet, T.-H. Chong, S. S. Apte, and N. Hogan, "Variable stiffness spring actuators for low-energy-cost human augmentation," *IEEE Transactions on Robotics*, vol. 35, no. 6, pp. 1435–1449, 2019.

[6] E. P. Grabke, K. Masani, and J. Andrysek, "Lower limb assistive device design optimization using musculoskeletal modeling: a review," *Journal of Medical Devices*, vol. 13, no. 4, 2019.

[7] E. P. Washabaugh, T. E. Augenstein, and C. Krishnan, "Functional resistance training during walking: Mode of application differentially affects gait biomechanics and muscle activation patterns," *Gait & Posture*, vol. 75, pp. 129–136, 2020.

[8] H. Su, W. Qi, Z. Li, Z. Chen, G. Ferrigno, and E. De Momi, "Deep neural network approach in emg-based force estimation for human–robot interaction," *IEEE Transactions on Artificial Intelligence*, vol. 2, no. 5, pp. 404–412, 2021.

[9] Z. Jin, A. Liu, W.-A. Zhang, L. Yu, and C.-Y. Su, "A learning based hierarchical control framework for human–robot collaboration," *IEEE Transactions on Automation Science and Engineering*, vol. 20, no. 1, pp. 506–517, 2022.

[10] K. Li, J. Zhang, L. Wang, M. Zhang, J. Li, and S. Bao, "A review of the key technologies for semg-based human-robot interaction systems," *Biomedical Signal Processing and Control*, vol. 62, p. 102074, 2020.

[11] S. Kim, J. Kim, M. Kim, S. Kim, and J. Park, "Grasping force estimation by semg signals and arm posture: tensor decomposition approach," *Journal of bionic engineering*, vol. 16, pp. 455–467, 2019.

[12] T. Yamasaki, K. Idehara, and X. Xin, "Estimation of muscle activity using higher-order derivatives, static optimization, and forward-inverse dynamics," *Journal of Biomechanics*, vol. 49, no. 10, pp. 2015–2022, 2016.

[13] Q. Shao, D. N. Bassett, K. Manal, and T. S. Buchanan, "An emg-driven model to estimate muscle forces and joint moments in stroke patients," *Computers in biology and medicine*, vol. 39, no. 12, pp. 1083–1088, 2009.

[14] J. W. Pau, S. S. Xie, and A. J. Pullan, "Neuromuscular interfacing: Establishing an emg-driven model for the human elbow joint," *IEEE Transactions on biomedical engineering*, vol. 59, no. 9, pp. 2586–2593, 2012.

[15] J. Hashemi, E. Morin, P. Mousavi, and K. Hashtrudi-Zaad, "Enhanced dynamic emg-force estimation through calibration and pci modeling," *IEEE Transactions on Neural Systems and Rehabilitation Engineering*, vol. 23, no. 1, pp. 41–50, 2014.

[16] C. Huang, X. Chen, S. Cao, B. Qiu, and X. Zhang, "An isometric muscle force estimation framework based on a high-density surface emg array and an nmf algorithm," *Journal of Neural Engineering*, vol. 14, no. 4, p. 046005, 2017.

[17] J. Zhang, Y. Zhao, F. Shone, Z. Li, A. F. Frangi, S. Q. Xie, and Z.-Q. Zhang, "Physics-informed deep learning for musculoskeletal modelling: Predicting muscle forces and joint kinematics from surface emg," *IEEE Transactions on Neural Systems and Rehabilitation Engineering*, 2022.

[18] Y. Zhao, J. Zhang, Z. Li, K. Qian, S. Q. Xie, Y. Lu, and Z.-Q. Zhang, "Computational efficient personalised emg-driven musculoskeletal model of wrist joint," *IEEE Transactions on Instrumentation and Measurement*, 2022.

[19] E. Dorschky, M. Nitschke, C. F. Martindale, A. J. Van den Bogert, A. D. Koelewijn, and B. M. Eskofier, "Cnn-based estimation of sagittal plane walking and running biomechanics from measured and simulated inertial sensor data," *Frontiers in bioengineering and biotechnology*, vol. 8, p. 604, 2020.

[20] W. R. Johnson, J. Alderson, D. Lloyd, and A. Mian, "Predicting athlete ground reaction forces and moments from spatio-temporal driven cnn models," *IEEE Transactions on Biomedical Engineering*, vol. 66, no. 3, pp. 689–694, 2018.

[21] M. F. Chaudhary, S. E. Gerard, D. Wang, G. E. Christensen, C. B. Cooper, J. D. Schroeder, E. A. Hoffman, and J. M. Reinhardt, "Single

volume lung biomechanics from chest computed tomography using a mode preserving generative adversarial network," in *2022 IEEE 19th International Symposium on Biomedical Imaging (ISBI)*. IEEE, 2022, pp. 1–5.

[22] J. Zhang, Y. Zhao, T. Bao, Z. Li, K. Qian, A. F. Frangi, S. Q. Xie, and Z.-Q. Zhang, "Boosting personalised musculoskeletal modelling with physics-informed knowledge transfer," *IEEE Transactions on Instrumentation and Measurement*, 2022.

[23] A. Nasr, S. Bell, J. He, R. L. Whittaker, N. Jiang, C. R. Dickerson, and J. McPhee, "Musclenet: mapping electromyography to kinematic and dynamic biomechanical variables by machine learning," *Journal of Neural Engineering*, vol. 18, no. 4, p. 0460d3, 2021.

[24] J. R. A. Solares, F. E. D. Raimondi, Y. Zhu, F. Rahimian, D. Canoy, J. Tran, A. C. P. Gomes, A. H. Payberah, M. Zottoli, M. Nazarzadeh *et al.*, "Deep learning for electronic health records: A comparative review of multiple deep neural architectures," *Journal of biomedical informatics*, vol. 101, p. 103337, 2020.

[25] M. N. Shadlen, K. H. Britten, W. T. Newsome, and J. A. Movshon, "A computational analysis of the relationship between neuronal and behavioral responses to visual motion," *Journal of Neuroscience*, vol. 16, no. 4, pp. 1486–1510, 1996.

[26] J. Holder, U. Trinler, A. Meurer, and F. Stief, "A systematic review of the associations between inverse dynamics and musculoskeletal modeling to investigate joint loading in a clinical environment," *Frontiers in bioengineering and biotechnology*, vol. 8, p. 603907, 2020.

[27] Y. Hu, A. Chapman, G. Wen, and D. W. Hall, "What can knowledge bring to machine learning?—a survey of low-shot learning for structured data," *ACM Transactions on Intelligent Systems and Technology (TIST)*, vol. 13, no. 3, pp. 1–45, 2022.

[28] S. Tam, M. Boukadoum, A. Campeau-Lecours, and B. Gosselin, "Siamese convolutional neural network and few-shot learning for embedded gesture recognition," in *2022 20th IEEE Interregional NEWCAS Conference (NEWCAS)*. IEEE, 2022, pp. 114–118.

[29] E. Rahimian, S. Zabihi, A. Asif, S. F. Atashzar, and A. Mohammadi, "Trustworthy adaptation with few-shot learning for hand gesture recognition," in *2021 IEEE International Conference on Autonomous Systems (ICAS)*. IEEE, 2021, pp. 1–5.

[30] E. Rahimian, S. Zabihi, A. Asif, D. Farina, S. F. Atashzar, and A. Mohammadi, "Fs-hgr: Few-shot learning for hand gesture recognition via electromyography," *IEEE transactions on neural systems and rehabilitation engineering*, vol. 29, pp. 1004–1015, 2021.

[31] S. J. Lehmler, M. Saif-ur Rehman, G. Tobias, and I. Iossifidis, "Deep transfer learning compared to subject-specific models for semg decoders," *Journal of Neural Engineering*, vol. 19, no. 5, p. 056039, 2022.

[32] I. J. Goodfellow, "On distinguishability criteria for estimating generative models," *arXiv preprint arXiv:1412.6515*, 2014.

[33] I. Goodfellow, J. Pouget-Abadie, M. Mirza, B. Xu, D. Warde-Farley, S. Ozair, A. Courville, and Y. Bengio, "Generative adversarial networks," *Communications of the ACM*, vol. 63, no. 11, pp. 139–144, 2020.

[34] Y. Shi, L. Han, L. Han, S. Chang, T. Hu, and D. Dancey, "A latent encoder coupled generative adversarial network (le-gan) for efficient hyperspectral image super-resolution," *IEEE Transactions on Geoscience and Remote Sensing*, vol. 60, pp. 1–19, 2022.

[35] Z. Chen, Y. Qian, Y. Wang, and Y. Fang, "Deep convolutional generative adversarial network-based emg data enhancement for hand motion classification," *Frontiers in Bioengineering and Biotechnology*, vol. 10, p. 909653, 2022.

[36] F. Fahimi, S. Dosen, K. K. Ang, N. Mrachacz-Kersting, and C. Guan, "Generative adversarial networks-based data augmentation for brain–computer interface," *IEEE transactions on neural networks and learning systems*, vol. 32, no. 9, pp. 4039–4051, 2020.

[37] J. Zhao, Y. Yu, X. Wang, S. Ma, X. Sheng, and X. Zhu, "A musculoskeletal model driven by muscle synergy-derived excitations for hand and wrist movements," *Journal of Neural Engineering*, vol. 19, no. 1, p. 016027, 2022.

[38] L. Yu, W. Zhang, J. Wang, and Y. Yu, "Seqgan: Sequence generative adversarial nets with policy gradient," in *Proceedings of the AAAI conference on artificial intelligence*, vol. 31, no. 1, 2017.

[39] Y. Han, R. Zhou, Z. Geng, K. Chen, Y. Wang, and Q. Wei, "Production prediction modeling of industrial processes based on bi-lstm," in *2019 34rd Youth Academic Annual Conference of Chinese Association of Automation (YAC)*. IEEE, 2019, pp. 285–289.

[40] S. Nah, T. Hyun Kim, and K. Mu Lee, "Deep multi-scale convolutional neural network for dynamic scene deblurring," in *Proceedings of the IEEE conference on computer vision and pattern recognition*, 2017, pp. 3883–3891.

[41] H. Wu, Y. Liu, and J. Wang, "Review of text classification methods on deep learning," *Comput. Mater. Contin*, vol. 63, no. 3, pp. 1309–1321, 2020.

[42] R. K. Srivastava, K. Greff, and J. Schmidhuber, "Highway networks," *arXiv preprint arXiv:1505.00387*, 2015.

[43] M. Q. Liu, F. C. Anderson, M. H. Schwartz, and S. L. Delp, "Muscle contributions to support and progression over a range of walking speeds," *Journal of biomechanics*, vol. 41, no. 15, pp. 3243–3252, 2008.

[44] Y. Zhao, Z. Zhang, Z. Li, Z. Yang, A. A. Dehghani-Sanij, and S. Xie, "An emg-driven musculoskeletal model for estimating continuous wrist motion," *IEEE Transactions on Neural Systems and Rehabilitation Engineering*, vol. 28, no. 12, pp. 3113–3120, 2020.

[45] N. Zhang, S. Ding, and J. Zhang, "Multi layer elm-rbf for multi-label learning," *Applied soft computing*, vol. 43, pp. 535–545, 2016.

[46] S. Solnik, P. DeVita, P. Rider, B. Long, and T. Hortobágyi, "Teager–kaiser operator improves the accuracy of emg onset detection independent of signal-to-noise ratio," *Acta of bioengineering and biomechanics/Wroclaw University of Technology*, vol. 10, no. 2, p. 65, 2008.

[47] L. Kahl and U. G. Hofmann, "Comparison of algorithms to quantify muscle fatigue in upper limb muscles based on semg signals," *Medical Engineering & Physics*, vol. 38, no. 11, pp. 1260–1269, 2016.

[48] L. Pan, K. Liu, and J. Li, "Effect of subcutaneous muscle displacement of flexor carpi radialis on surface electromyography," *IEEE Transactions on Neural Systems and Rehabilitation Engineering*, vol. 30, pp. 1244–1251, 2022.

[49] S. Jung and M. Keuper, "Internalized biases in fréchet inception distance," in *NeurIPS 2021 Workshop on Distribution Shifts: Connecting Methods and Applications*, 2021.